

Multiferroicity in the spin-1/2 quantum matter of LiCu_2O_2

A. Rusydi, I. Mahns, S. Müller, and M. Rübhausen

Institut für Angewandte Physik, Universität Hamburg, Jungiusstraße 11, D-20355 Hamburg, Germany

S. Park, Y.J. Choi, C. L. Zhang, and S-W. Cheong

Department of Physics & Astronomy, Rutgers University, Piscataway, New Jersey 08854, USA

S. Smadici, P. Abbamonte

Physics Department and Frederick Seitz Materials Research Laboratory, University of Illinois, Urbana, IL, 6180, USA

M. v. Zimmermann

Hamburger Synchrotronstrahlungslabor HASYLAB at Deutsches Elektronen-Synchrotron DESY, Notkestraße 85, 22603 Hamburg, Germany

G. A. Sawatzky

Department of Physics and Astronomy, University of British Columbia, Vancouver, British Columbia V6T-1Z1, Canada

Multiferroicity in LiCu_2O_2 single crystals is studied using resonant soft x-ray magnetic scattering, hard x-ray diffraction, heat capacity, magnetic susceptibility, and electrical polarization. Two magnetic transitions are found at 24.6 K (T_1) and 23.2 K (T_2). Our data are consistent with a sinusoidal spin structure at $T_2 < T < T_1$ and with a helicoidal spin structure at $T < T_2$ giving rise to ferroelectricity. Surprisingly, above T_2 the correlation lengths of the spin structures increase as the temperature increases with dramatic changes of $\sim 42\%$ along the c -axis. Our results demonstrate the interplay of the geometrical frustration and the electronic and magnetic polarizations.

Low-dimensional spin (S)=1/2 systems have posed some of the most challenging scientific questions in solid state physics. The interplay between frustration and quantum spin fluctuations results in a rich phase diagram and unusual magnetic properties. In a model with quantum $S=1/2$ chains and competing nearest-neighbor interactions J_1 and next-nearest-neighbor interactions J_2 , one expects, depending on J_1/J_2 , a gapless collinear phase, a gapped disordered dimer liquid phase, or a quasi-long-range ordered helicoidal spin structure.¹

In **Fig. 1(a)**, LiCu_2O_2 consists of an equal number of Cu^{1+} and Cu^{2+} . The magnetic Cu^{2+} ions carry $S=1/2$ and are located at the center of edge-sharing CuO_4 plaquettes and form two frustrated quasi-one dimensional (1D) $S=1/2$ chains along the b -axis. These chains are separated by Li^{1+} ions to form double layers parallel to the ab -plane which are separated by Cu^{1+} sites. Within each chain, the Cu-O-Cu angle is about 94° . As a result J_2 is weaker than J_1 . The strength of the interaction between chains (J_{DC}) is not clear, however we expect J_1 to be ferromagnetic and J_2 to be antiferromagnetic based on analysis of the magnetic susceptibility $\chi(T)$.² This leads to frustration and favors helimagnetism.¹ A similar scenario was recently proposed for a very similar isostructural NaCu_2O_2 .³

LiCu_2O_2 exhibits striking properties such as the presence of a spin-singlet liquid state⁴, incommensurate (IC) magnetic order⁵ as well as ferroelectricity.⁶ However, all these properties are not well-understood. One problem is the intrinsic chemical disorder. Electron-spin resonance (ESR)⁴ has shown the presence of a spin-singlet state with a spin gap of 6 meV at 23 K. Specific heat⁴ and nuclear magnetic resonance (NMR)⁷ show phase transitions at 24.2 K, 22.5 K, and 9 K. Recent neutron diffraction⁵ found one transition to an incommensurate (IC) magnetic superstructure below 22 K with a propagation vector $Q=(\frac{[2n+1]}{2}, k+\delta, l)$ where n , k , and l are integer and $\delta \sim 0.174$. Thus it is concluded that the magnetic superstructure is a helical in the ab -plane. This is inconsistent with the observation of ferroelectricity with an electric polarization along the c -direction below ~ 23 K.⁶

In an attempt to understand the coupling between lattice, charge, and spin degrees of freedom in $S=1/2$ quantum systems, we have studied a LiCu_2O_2 single crystal using polarization-dependent resonant soft x-ray magnetic scattering (RSXMS), hard x-ray diffraction (HXD), heat capacity, magnetic susceptibility, and electrical polarization. All experiments were done on the same sample.

The LiCu_2O_2 single crystal was grown by the self-flux method.⁶ The HXD was done at the BW5 beamline of HASYLAB (DESY) with a photon energy of 100.5 keV. The lattice parameters of the orthorhombic structure at 10 K are $a=5.6963$, $b=2.8497$, and $c=12.417$ Å. The HXD highlights the high crystalline perfection and confirms the absence of crystalline impurity phases. The crystal is found to be microscopically twinned along the $[1,1,0]$ plane with $a \sim 2b$. Below 23 K (T_{FE}), LiCu_2O_2 becomes ferroelectric (FE) and shows a small anomaly in the dielectric constant ϵ .⁶ **Figure 2(b)** shows a changing dielectric polarization (P) along the c direction as function of

temperature. However, the observed polarization ($\sim 4\mu\text{C}/\text{m}^2$) is smaller by 2-3 orders of magnitude as compared to RMnO_3 ^{8,9} and RMn_2O_5 .^{9,10}

Two magnetic transitions are found in the magnetic susceptibility, χ (**Fig. 2(a)**). For an applied magnetic field H parallel to the c -axis ($H\parallel c$), the curve $d\chi_c/dT$ presents transitions, at 23.2 K (T_2) and 24.6 K (T_1), while for $H\parallel b$, the $d\chi_c/dT$ shows only a sharp transition at 23 K. The T_2 coincides with T_{FE} from heat capacity measurements (**Fig. 2(a)**). Our sample does not show any other transition below 23 K.¹¹

RXSMS was done on a surface which was cleaved *in-situ* with (2,1,0) orientation at the beamline X1B of the National Synchrotron Light Source (Brookhaven) using a 10-axis, ultrahigh-vacuum-compatible diffractometer.^{12,13} X-ray absorption spectra (XAS) were measured in-situ in the fluorescence yield mode at the $\text{Cu}L_{3,2}$ edges. We denote the reciprocal space with Miller indices (H, K, L), which represent a momentum transfer $\mathbf{Q} = (2\pi H/a, 2\pi K/b, 2\pi L/c)$. The angle of incoming (θ_{in}) and outgoing photons (θ_{out}) depends on \mathbf{Q} but was approximately 35° and 55° , respectively. The azimuthal angle, ϕ , is $\phi=0^\circ$ and 90° (**Fig. 1(b)**).

Scattering at transition metal L edges is known to be sensitive to the spin modulation.^{14,15,16,17} **Figure 1 (c)** illustrates $\text{Cu } 2p \rightarrow 3d$ resonant scattering process which enhances the magnetic scattering from Cu^{2+} . In the cuprate systems, the $\text{Cu } 2p \rightarrow 3d$ transition exhibits two main peaks corresponding to final states with $2p_{3/2}$ and $2p_{1/2}$ core holes, referred to as the $\text{Cu}L_3$ and $\text{Cu}L_2$ absorption edges, respectively. This material is particularly interesting because it has a clear contrast in the scattering of the Cu^{1+} and Cu^{2+} sites (see **Fig. 2(d)**). The peaks at 930 eV and 950 eV are $\text{Cu}L_{3,2}$ edges of Cu^{2+} sites and the peaks at 933 eV and 953 eV are $\text{Cu}L_{3,2}$ edges of Cu^{1+} sites.¹⁸

Probing with a photon energy $E = 930$ eV, an IC superstructure with $\mathbf{Q} = (0.5, 0.1738, 0)$ at $T = 18$ K is observed (**Fig. 2(c)**). This is identical to the magnetic superstructure found by neutron diffraction.⁵ Our experiment reveals that the correlation lengths along a , b , and c are very large with $\xi_a=(1662\pm 20)$, $\xi_b=(2120\pm 20)$, and $\xi_c=(935\pm 20)$ Å, respectively. X-rays at 930 eV have penetration depth of 2500 Å.

Figure 2(d) shows the scattering intensity of the superstructure (I_{ss}) as a function of photon energy, i.e. the resonance profile (RP), at 18 and 24.6 K across the $\text{Cu}L_3$ edge. The 24.6 K and 18 K measurements show magnetic scattering above and below the FE transition, respectively. The RP is compared to the complex atomic scattering factor of Cu^{2+} , $f_{\text{Cu}}(E)$. In this case, $I_{ss} \propto |f_{\text{Cu}}|^2 = |\text{Re}[f_{\text{Cu}}] + i\text{Im}[f_{\text{Cu}}]|^2$. The $\text{Im}[f_{\text{Cu}}(E)]$ is determined from the absorptive part of the refractive index, $\text{Im}[n]$, which is linearly related to the XAS spectrum, through the relation $\text{Im}[n(E)] = -(r_e \lambda^2 N / 2\pi V_{\text{cell}}) \text{Im}[\sum_i f_i(E)]$. The $\text{Re}[f_{\text{Cu}}(E)]$ is calculated from $\text{Im}[f_{\text{Cu}}(E)]$ by performing a Kramers-Kronig transform. Here r_e is the classical electron radius, λ is the x-ray wavelength, N is the number of Cu in the unit cell, and f_i is the complex atomic scattering factor. The XAS measurement was done with an incident x-ray polarization in the ab -plane, at room temperature, corrected for self absorption, and placed on an absolute scale.¹⁹ It is clear that the superstructure is greatly enhanced at the Cu^{2+} peak. A gigantic enhancement occurs in the

magnetic-*FE* state. In a soft x-ray measurement a superstructure due to a lattice distortion would result in orders of magnitude smaller scattering intensities.¹²

We have performed a HXD study to rule out a lattice modulation.²⁰ Even at 4 K, neither a $(0.5, k \pm \delta, 0)$ nor a $(0.5, k \pm 2\delta, 0)$ reflection was found supporting that the lattice distortion is extremely small. This is in contrast to ferroelectric TbMnO_3 in which lattice distortions are observed.²¹ This further supports the conclusion that the lattice related effects are very weak.

Figure 3(a) and **3(b)** display the intensity together with position of the Bragg peak as a function of temperature and the polarization of the incoming photon. For $\phi=0^\circ$, we have found the presence of two magnetic transitions: at ~ 23.2 K and ~ 24.6 K which is consistent with the magnetic susceptibility. The intensity increases as the temperature decreases indicating an enhanced magnetic order upon cooling, while Q also changes with temperature. For $\phi=90^\circ$, the superstructure vanishes rapidly above T_2 .

The combination of polarization-dependent RSXMS, HXD, magnetic susceptibility, and the electrical polarization measurements provides crucial information regarding the coexistence of *FE* and magnetic states. At $T_2 < T < T_1$, we find: First, $d\chi/dT$ shows an anomaly at T_1 for $H||c$ implying that the c -direction is an *easy* axis (**Fig. 2(a)**); Second, there is no *FE*, i.e. $P = 0$ (**Fig. 2(b)**); Third, for $\phi=0^\circ$ RSXMS experiment shows a magnetic Bragg reflection while for $\phi=90^\circ$ the superstructures is very weak. For spins which have a component of the magnetic moment along the c -axis, the polarization factor of the magnetic scattering $f_{mag} = (\vec{e}_{in} \times \vec{e}_{out}) \cdot \hat{\mathbf{M}} \neq 0$. This implies that the spins have a strong component or are oriented along the c -axis; Fourth, no harmonics and no lattice distortion were found at $Q = 2\delta$. A helical structure in ac -plane would result in a polarization independence. Therefore, we propose that the spin structure is a sinusoidal with the spin oriented along the c -axis and propagating with Q along the b -direction.

For $T < T_2$ we find: First, $d\chi/dT$ shows the magnetic transitions for $H||b$ and $H||c$ implying that b and c are both the easy axis (**Fig. 2(b)**); Second, *FE* is present with $P_c \approx 3 \mu\text{C}/\text{m}^2$ (**Fig. 3(a)**); Third, f_{mag} is non-zero for $\phi=0^\circ$ and 90° , giving rise to a magnetic Bragg reflection; Fourth, no harmonics and no lattice distortion are found at $Q = 2\delta$. These results cannot be explained with a simple spiral spin structure in the bc -plane as such a condition would result in $f_{mag}=0$ for $\phi=90^\circ$. A pure helical or sinusoidal spin wave cannot cause ferroelectricity since $\mathbf{P} \cdot \nabla \mathbf{M}$ is zero.²² Therefore, our results are consistent with a spin structure that is helicoidal having a , b , and c components, and propagating with Q along the b direction. The complexity of the helicoidal structure relates to a coupling of the two frustrated quasi-1D $S=1/2$ chains along the b -axis, as shown in **Fig. 1(a)**, resulting to a total polarization P along the c -axis. This highlights the underlying frustration. Frustration can be lifted by breaking the symmetry yielding an electronically driven ferroelectric order.

Moreover, we find a decreased correlation length in the *FE* state with decreasing temperature [see **Fig. 3(c)-(e)**]. A dramatic change of the coherence lengths occurs around T_2 which is the transition from sinusoidal to helicoidal spin structures. The strongest change is $\sim 42\%$ along c ,

followed by ~22% along b , and ~4% along the a directions. The strongest distortion is along the c direction which is also the direction of the ferroelectric moment. This is a surprising result as it cannot be explained by enhanced thermal fluctuations close to the phase transition. Usually, the correlation lengths are getting shorter at high temperatures due to fluctuations which eventually destroy the long range order. In our case, FE domains form below T_2 in the helicoidal spin phase disturbing the magnetic coherence lengths while the sinusoidal spin structure above T_2 is free of FE domains leading to an increased coherence length with increasing temperature.

Another interesting observation is the smallness of the temperature *window* between the two transitions. In $TbMnO_3$, $S=2$,²⁰ the temperature window is about 12 K. In the spinel $CoCr_2O_4$, $S=3$ ²³ the temperature window is ~65K. This shows that the lack of a single ion magnetic anisotropy in $S=1/2$ systems results in an unstable sinusoidal phase supporting our picture of an electronically driven phase. Related to this is the increased coherence lengths with increasing temperature above T_{FE} indicating remaining dynamic FE domain ordering.

In conclusion, we have found two magnetic transitions in $LiCu_2O_2$: a sinusoidal spin structure at $T_2 < T < T_1$ and a helicoidal spin structure at $T < T_2$ giving rise to ferroelectricity. The coherence lengths of the superstructure are increasing as the temperature increases. We understand these phenomena by considering the interplay between magnetic and electronic ordering.

We acknowledge M. Mostovoy for helpful discussions and financial support by the Helmholtz Association VH-FZ-007, DFG Ru 773/2-3, DOE No. DE-FG02-06ER46285, NSLS No. DE-AC02-98CH10886, NSF-MDR-0405682, NSERC, CIAR, and CFI.

-
- [1] R. A. Erickson, Phys. Rev. **85**, 745 (1952); A. Yoshimori, J. Phys. Soc. Jpn. **14**, 807 (1959).
- [2] S.-L. Drechsler, J. Málek, J. Richter, A. S. Moskvin, A. A. Gippius, and H. Rosner, Phys. Rev. Lett. **94**, 039705 (2005).
- [3] L. Capogna, M. Mayr, P. Horsch, M. Raichle, R. K. Kremer, M. Sofin, A. Maljuk, M. Jansen, and B. Keimer, Phys. Rev. B **71**, 140402(R) (2005).
- [4] S. Zvyagin, G. Cao, Y. Xin, S. McCall, T. Caldwell, W. Moulton, L.-C. Brunel, A. Angerhofer, and J. E. Crow, Phys. Rev. B **66**, 064424 (2002).
- [5] T. Masuda, A. Zheludev, A. Bush, M. Markina, and A. Vasiliev, Phys. Rev. Lett. **92**, 177201 (2004).
- [6] S. Park, Y. J. Choi, C. L. Zhang, and S-W. Cheong, Phys. Rev. Lett. **98**, 057601 (2007).
- [7] A. A. Gippius, E. N. Morozova, A. S. Moskvin, A. V. Zalessky, A. A. Bush, M. Baenitz, H. Rosner, and S.-L. Drechsler, Phys. Rev. B **70**, 020406(R) (2004).
- [8] T. Kimura, G. Lawes, T. Goto, Y. Tokura, and A. P. Ramirez, Phys. Rev. B **71**, 224425 (2005).
- [9] S-W. Cheong & M. Mostovoy, Nature Materials **6**, 13 (2007).
- [10] N. Hur, S. Park, P. A. Sharma, J. S. Ahn, S. Guha, and S-W. Cheong, Nature **429**, 392 (2004).
- [11] E. M. L. Chung, G. J. McIntyre, D. McK. Paul, G. Balakrishnan, and M. R. Lees, Phys. Rev. B **68**, 144410 (2003).
- [12] P. Abbamonte, L. Venema, A. Ruydi, G. A. Sawatzky, G. Logvenov, I. Bozovic, Science **297**, 581 (2002)
- [13] A. Ruydi, Resonant soft x-ray scattering and charge density waves in strongly correlated systems, PhD thesis, Rijkuniversiteit Groningen (2006).
- [14] C. Kao, J. B. Hastings, E. D. Johnson, D. P. Siddons, and G. C. Smith, and G. A. Prinz, Phys. Rev. Lett. **65**, 373 (1990).

-
- [15] H. A. Dürr, E. Dudzik, S. S. Dhesi, J. B. Goedkoop, G. van der Laan, M. Belakhovsky, C. Mocuta, A. Marty, and Y. Samson, *Science* **284**, 2166 (1999).
- [16] K. J. Thomas, J. P. Hill, S. Grenier, Y.-J. Kim, P. Abbamonte, L. Venema, A. Rusydi, Y. Tomioka, Y. Tokura, D. F. McMorrow, G. Sawatzky, and M. van Veenendaal, *Phys. Rev. Lett.* **92**, 237204 (2004).
- [17] C. Schüßler-Langeheine, J. Schlappa, A. Tanaka, Z. Hu, C. F. Chang, E. Schierle, M. Benomar, H. Ott, E. Weschke, G. Kaindl, O. Friedt, G. A. Sawatzky, H.-J. Lin, C. T. Chen, M. Braden, and L. H. Tjeng, *Phys. Rev. Lett.* **95**, 156402 (2005).
- [18] L. H. Tjeng, C. T. Chen, and S.-W. Cheong, *Phys. Rev. B* **45**, 8205 (1992).
- [19] B.L. Henke, E.M. Gullikson, and J.C. Davis, *Atomic Data and Nuclear Data Tables* **54**, 181 (1993).
- [20] T. Kimura, T. Goto, H. Shintani, K. Ishizaka, T. Arima, and Y. Tokura, *Nature* **426**, 55 (2003)
- [21] N. Aliouane, D. N. Argyriou, J. Strempler, I. Zegkinoglou, S. Landsgesell, and M. v. Zimmermann, *Phys. Rev. B* **73**, 020102(R) (2006).
- [22] M. Mostovoy, *Phys. Rev. Lett.* **96**, 067601 (2006).
- [23] Y. Yamasaki, S. Miyasaka, Y. Kaneko, J.-P. He, T. Arima, and Y. Tokura, *Phys. Rev. Lett.* **96**, 207204 (2006).

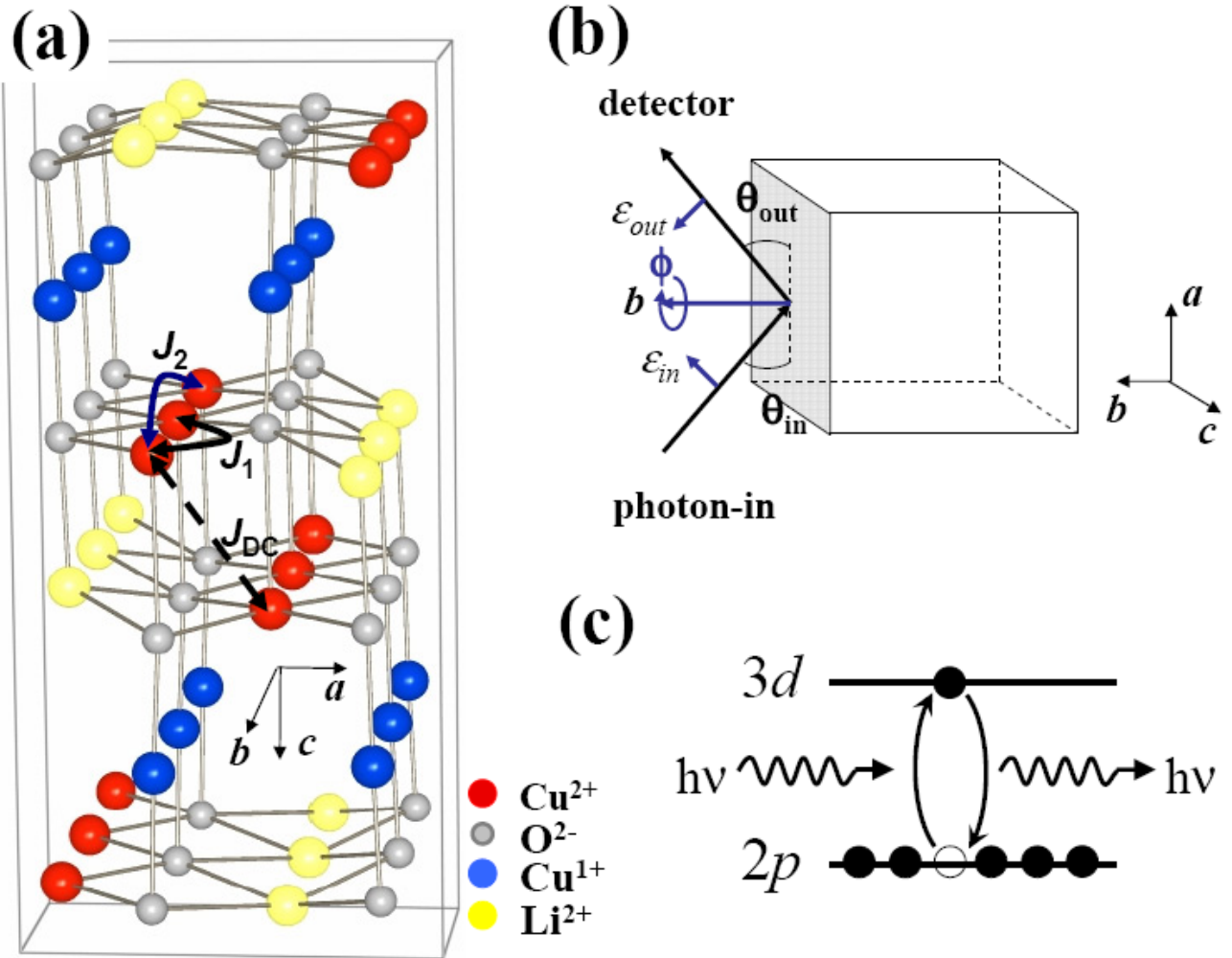


Figure 1. (a) The crystal structure of LiCu_2O_2 and the double chains showing J_1 , J_2 and J_{DC} . (b) The scattering experimental geometry with photon polarization ϵ in the scattering plane. The azimuthal angle, ϕ , is 0° in the geometry shown, where the photon polarization is perpendicular to c -axis. (c) An illustration of $\text{Cu } 2p \rightarrow 3d$ resonant scattering process.

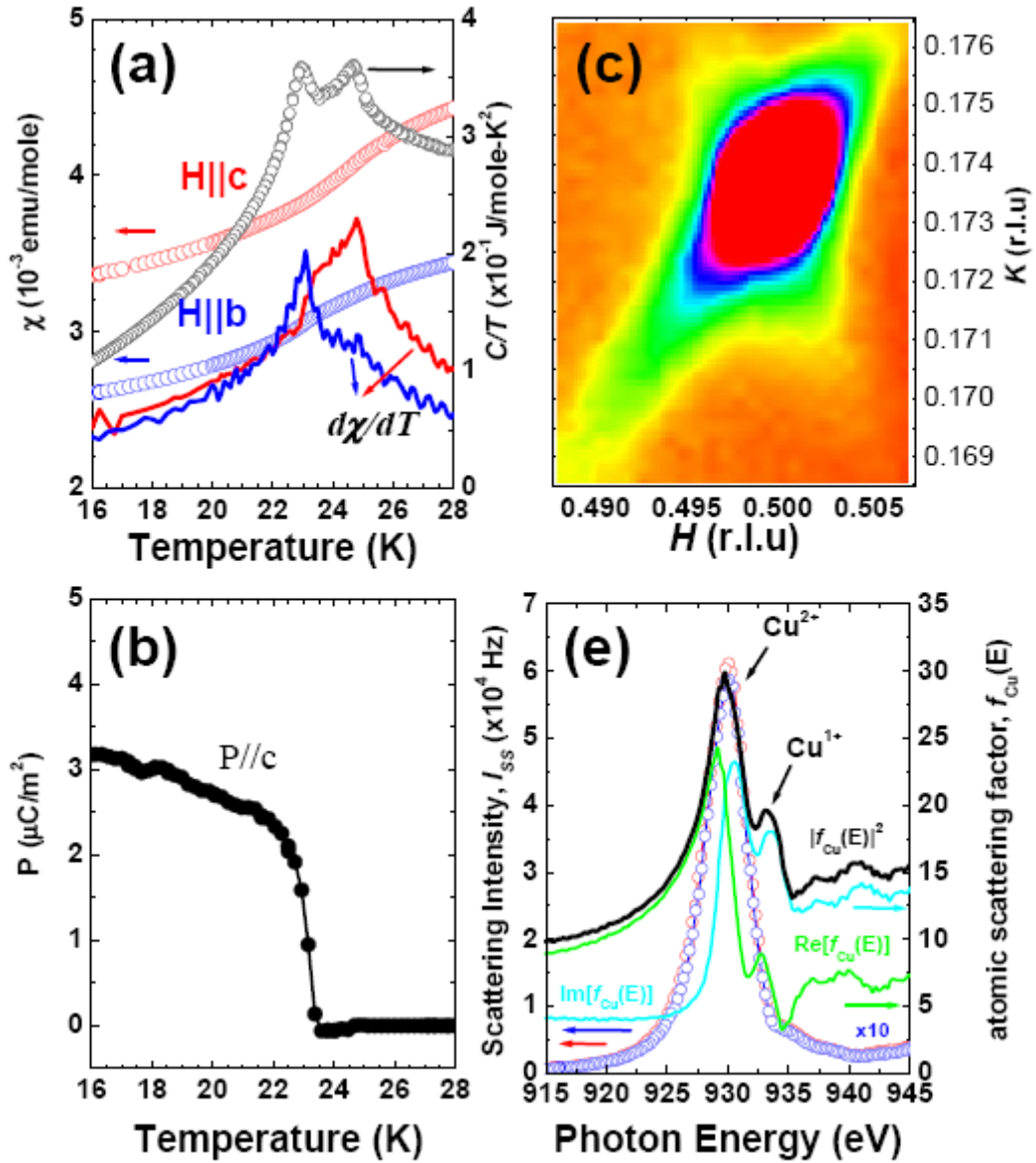


Figure 2. (a) magnetic susceptibility and heat capacity measurements showing two magnetic transitions, at 23.2 K and 24.6 K. (b) The electrical polarization changes along c -axis showing the onset of polarization at 23.2 K. (c) Appearance of the magnetic structure on resonance ($E=930$ eV) in the reciprocal space map $(H,K,L) = (0.5, 0.174, 0)$ taken at 18 K. The correlation length along n direction, ξ_n is defined as $n_n/\Delta q_n$, where Δq_n is the width of the Bragg reflection and n_n is the lattice parameter along n direction. (d) Energy scan at fixed- $Q = (0.5, \delta, 0)$ for two different temperatures: 18 K at $\delta=0.1738$ (red dots) and 24.6 K at $\delta=0.1722$ (blue dots) showing the same profile which indicates the lack of lattice distortion in the FE phase ($T_{FE} = 23.2$ K) at this particular and direction of modulation. The energy dependence of the resonantly diffracted intensity is compared to the complex atomic scattering factor of Cu, $f_{Cu}(E)$, to highlight the resonant the Cu^{2+} peak.

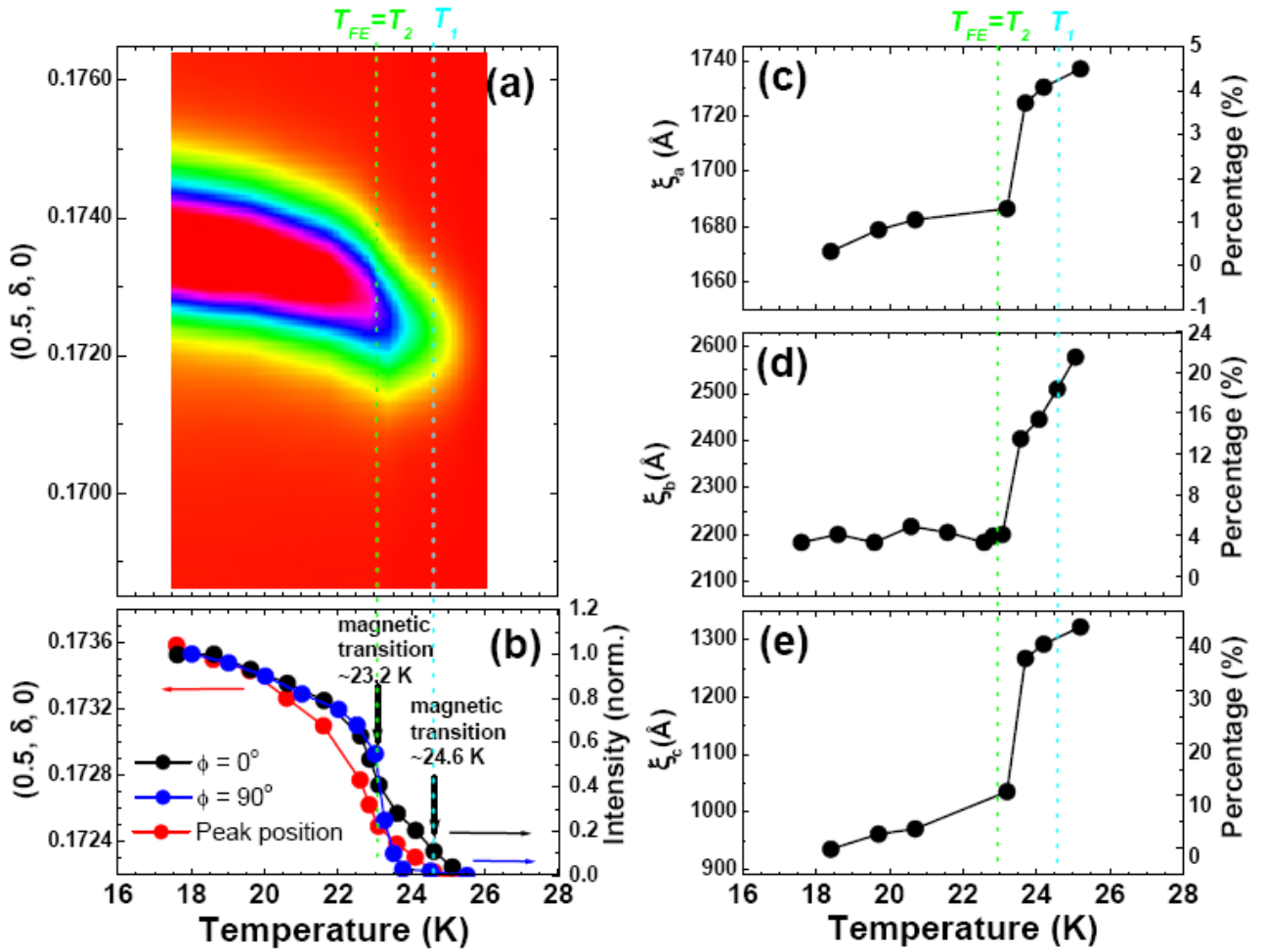


Figure 3. (a) Two-dimensional plot of temperature vs $(0.5, K, 0)$ for $\phi=90^\circ$ showing the changing of peak position as function of temperature. (b) The evolution of the (red dots) peak position, δ and (black and blue dots) intensity of the magnetic scattering for the two polarizations as function of temperature showing two transitions: ~ 23.2 K and ~ 24.6 K. (c)-(e) Correlation lengths of the magnetic ordering at the transition into the FE state for all crystallographic directions.